A power-balance model of the density limit in fusion plasmas: application to the L-mode tokamak

Original
A power-balance model of the density limit in fusion plasmas: application to the L-mode tokamak / Zanca, P.; Sattin, F.; Escande, D. F.; Subba, F.. - In: NUCLEAR FUSION. - ISSN 0029-5515. - 59:12(2019). [10.1088/1741-4326/ab3b31]

Publisher:
IOP Publishing Ltd

Published
DOI:10.1088/1741-4326/ab3b31

A POWER-BALANCE MODEL OF DENSITY LIMIT IN FUSION PLASMAS: APPLICATION TO THE L-MODE TOKAMAK

P. Zanca, F. Sattin
Consorzio RFX (CNR, ENEA, INFN, Università di Padova, Acciaierie Venete Spa)
Padova, Italy.
Email: paolo.zanca@igi.cnr.it

D. F. Escande
Aix-Marseille Université, CNRS, PIIM, UMR 7345
Marseille, France.

JET Contributors: see the author list of "X. Litaudon et al 2017 Nucl. Fusion 57 102001"

Abstract

A power-balance model, with radiation losses from impurities and neutrals, gives a unified description of density limit of the stellarator, the L-mode tokamak, and the Reversed Field Pinch (RFP). The model predicts a Sudo-like scaling for the stellarator, a Greenwald-like scaling, $\propto I_p^{8/9}$, for the RFP and the ohmic tokamak; a mixed scaling, $\propto P^{4/9} I_p^{4/9}$, for the additionally heated L-mode tokamak. In a previous paper [P. Zanca et al, Nucl. Fusion **57** (2017) 056010] the model has been compared with ohmic tokamak, RFP and stellarator experiments. Here, we address the issue of the density limit dependence on heating power in the L-mode tokamak. Experimental data from high-density disrupted L-mode discharges performed at JET, as well as in other machines, are taken as term of comparison. The model fits the observed maximum densities much better than the pure Greenwald limit.

1. Introduction

A density limit (DL), causing either a disruption or a soft termination of the discharge, is generally found in magnetic confinement fusion devices. Some empirical scaling laws have been proposed for the maximum achievable densities. The Sudo limit, $n_{Sudo}(10^{20} m^{-3}) = 0.25 \times \left[P(MW)\, B_\phi/(R_0\, a^2)\right]^{0.5}$ [1], with P the total heating power, R_0, a the major and minor radii of the device respectively (all quantities in SI units), is generally applied to the stellarator. The Greenwald density, $n_G(10^{20} m^{-3}) = I_p(MA)/(\pi a^2)$, with I_p the plasma current, is a reference for the tokamak [2] and the Reversed Field Pinch (RFP) [3]: a remarkable feature in view of the differences between these two configurations, both in terms of magnetic profiles and transport properties. Nonetheless, additionally heated tokamak experiments in L-mode suggest a weaker dependence on current alongside an explicit power dependence: $\sim I_p^{0.5} \times P^{0.3 \div 0.5}$ [4, 5]. This power dependence is observed at JET in L-mode independently of the wall material [6]. The tokamak H-mode DL, identified by a back transition to L-mode, looks as more device dependent: in particular, no dependence on P is found in [7], whereas a dependence $P^{0.4}$ is obtained in [8]. However, since this transition is generally not disruptive, the discharge-terminating (ultimate) DL of tokamaks pertains to the L-mode.

The possible origin of the ultimate DL from some basic mechanism, weakly sensitive to the details of the configuration, is an intriguing concept. However, this collides with the diversity of the above-mentioned empirical relations, in particular as far as the Greenwald and the Sudo limits are concerned. The power-balance analytical model model presented in [9] provides a way to solve this contradiction. In fact, scaling laws resembling the above empirical trends, but richer in their parametric dependence, are derived as special cases of a more fundamental relation, which delimits the thermal equilibrium states having realistic temperature profiles (i.e. with low temperature only at the edge) in the presence of radiation losses. Hence, the empirical scaling laws would be approximate relations, whereas only the model discloses all the important dependences, with scaling laws that are *correct dimensionally*. As far as the tokamak is concerned, the scaling laws so obtained should be representative of the L-mode, since the pedestal physics ruling the H-mode, is not included in this basic model.

In this paper, an improved version of the model [9] is presented, featuring, in particular, two refinements. 1) The previous analysis considered radiation from the plasma edge only, approximation justified for a plasma polluted by light impurities, which radiate mostly at low temperature. The new version is more general, since it also takes into account radiation from the plasma bulk, which is particularly important in the presence of heavy impurities. Moreover, radiation from edge neutral particles is included. 2) In [9], the transport dependence of the DL scaling laws was given in terms of the edge thermal conductivity. Here, this dependence is expressed by the global energy confinement time τ_E, which is a quantity easily retrievable from experimental databases. The final DL scaling laws contains some terms, most of them related to profile effects, whose evaluation is not straightforward. Therefore, we also present, limited to the L-mode Tokamak, a reduced, more manageable scaling, where these terms are replaced by suitable average numerical factors.

In [9] the model has been validated by considering published data from ohmic tokamak, RFP and stellarator experiments. Here we focus on the L-mode tokamak, addressing, in particular, the dependence on the heating power. In fact, according to the model, the heating power is as important as the current and the emitting species concentration, for the L-mode tokamak. To this purpose, a database of high-density disrupted L-mode discharges performed at JET is analysed. With respect to the previous validation [9], we take advantage of shot-by-shot signals for most of the needed quantities. It turns out that the model fits fairly well the maximum densities, whereas the pure Greenwald limit does not work at all. We get the same result, when our model and the Greenwald limit are compared to published data of L-mode experiments from several tokamaks.

The paper is organized as follows. In section 2 the new version of the model is presented. Section 3 is devoted to the analysis of the JET database. In Section 4 the reduced DL scaling law is derived and compared to the JET database, as well as to published results from other devices. Section 5 criticizes to the arguments brought by [2] to support the independence from power of the L-mode tokamak DL. Conclusions are drawn in section 6. More technical issues are moved to the appendixes: atomic data, appendix A; estimate of profile terms, appendix B; derivation of scaling (17), appendix C; approximate relationship between the edge temperature and its gradient, appendix D.

stellarator	$(n_e)_{DL} \propto P^{0.57}\, B_\phi^{0.33}\, R_0^{-0.54}\, a^{-0.72}\, \hat{G}_*^{-0.4}$	Eq. (12)
RFP & ohmic tokamak	$(n_e)_{DL} \propto Z_{eff}^{\frac{4}{9}}\, \hat{G}_*^{-\frac{5}{9}}\, \tau_E^{-\frac{1}{9}}\, n_G^{\frac{8}{9}}$	Eq. (17)
L-mode tokamak: reduced scaling from Eq. (17)	$(n_e)_{DL} \propto Z_{eff}^{\frac{4}{9}}\, \hat{G}_*^{-\frac{5}{9}}\, (P/I_P)^{\frac{4}{9}}\, n_G^{\frac{8}{9}}$	Eq. (20)

Table I. Summary of DL scaling laws predicted by the model: $\hat{G}_*$ is an edge factor for the emitting species, explained in more detail in the text.

For the reader's convenience we provide in Table I a quick summary of the model's scaling laws for the different configurations, where we dropped profile terms, as well as global numerical factors, for the sake of simplicity. Quantity $\hat{G}_*$ encapsulates means edge values for the concentration and the radiation rate coefficient of both impurities and neutral particles, and Z_{eff} is the plasma effective charge. Here are a few comments about the above scaling laws. Equation (12) is a Sudo-like expression for the stellarator. For the RFP and the ohmic tokamak, scaling (17) turns out to be quantitatively very similar, thanks to the negligible dependence on the energy confinement time ($\tau_E^{-1/9}$), and in both cases it features the quasi-linear dependence $n_G^{8/9}$. For the additionally heated tokamak, the overall dependence on power and current of (17) is $P^{4/9}\, I_p^{4/9}$: in equation (20), reported in the Table, we present a reduced form of (17) for this configuration, obtained by replacing some terms with suitable numerical factors. The reader may skip the somewhat long section 2, and move directly to figures 2, 7, 8 to take a view of how scaling (20) and the customary Greenwald limit compare with several L-mode tokamak experiments.

2. The model

As explained in the introduction the new derivation of the DL scaling laws involves two useful improvements, but is very similar to that discussed in [9]. The starting point is the same: a phenomenological equation describing thermal balance in cylindrical geometry. This is obtained by summing together the heat transport equations for electrons and main ions, thus removing their energy exchange term, and neglecting convection as well as viscous heating [10]:

$$1)\ \frac{d}{dr}\left(r\,K\,\frac{dT}{dr}\right)+r(\wp-\Re)\ =0;\qquad \Re=\ n_e^2\left[\sum_j f_j Rad_j\,(T)+f_0 Rad_0(T)+Rad_i(T)\right]$$

Here, T is the electron temperature; K is an *effective* perpendicular conductivity, which includes the main ion contribution to the heat flux [9]. The radial functions $\wp(r),\ \Re(r)$ are respectively the heating power density (with ohmic and auxiliary components) and the radiated power density. Moreover, n_e is the electron density; f_j, Rad_j are the *j-th* impurity concentration and radiation rate coefficient respectively; f_0, Rad_0 are the same quantities for neutrals. Finally, Rad_i is the main ion radiation rate coefficient, a minor effect in the here considered plasmas. The impurity concentrations are allowed to vary with *r*, but the concentrations relative to the dominant impurity (denoted by *d*), $\hat{f}_j=f_j/f_d$, *are assumed to be radially constant*. Throughout this paper we use the International System of units (SI), but for the temperature, which is expressed in keV. Therefore, K incorporates the numerical factor 1.6×10^{-16}. The temperature profile satisfies the symmetry condition $T'(0)=0$ ($'\equiv d/dr$). Moreover, the request of ambient temperature value at $r=a$, location of the first material wall, is modelled by the constraint $T(a)=0$.

For light impurities Rad_j has a principal maximum in the tens eV temperature range, followed by a secondary maximum in the few hundreds eV range (see estimates in figure A1 of appendix A). We distinguish a low temperature interval $T<T_*$ where emission from light impurities is important, from the complementary interval $T>T_*$. The separation radius r_*, defined by $T(r_*)=T_*$, is assumed to be *uniquely determined* and *close to the wall*: $r_*\approx a$. Given the smallness of T_*, namely $T_*\lesssim 0.1\div 0.2keV$, any realistic temperature profile should fulfil this constraint. Note that, in this cylindrical model the scrape-off-layer (SOL) of a real experiment is included within the edge region $[r_*,\ a]$.

It is convenient defining an *impurity-average radiation rate coefficient* F, such that $\sum_j f_j Rad_j=\left(Z_{eff}-Z_i\right)\times F$, with Z_{eff} the plasma effective charge and Z_i the main ion charge. In addition to the temperature, F is a function of the *constant* parameters $\hat{f}_j$ only. In fact, from the relationship $Z_{eff} - Z_i = \sum_j f_j \left(Z_j^2 - Z_j Z_i\right)$, with $Z_j(T)$ the *j-th* impurity charge, one gets

$$2) \quad F(T, \hat{f}_j) = \sum_j \hat{f}_j Rad_j(T) / \sum_j \hat{f}_j \left[Z_j^2(T) - Z_j(T) Z_i\right].$$

Note that, with the representation $\sum_j f_j Rad_j = \left(Z_{eff} - Z_i\right) \times F$ all the information about f_j are supplied by $\hat{f}_j$, Z_i and Z_{eff}. In particular, Z_{eff} is taken *radially constant*, an approximation compatible with many experimental observations.

The modelling of neutral radiation is more problematic, since the distribution of these particles is highly localized both radially (at the very edge) and poloidally (in the divertor region, if present). Dealing with a cylindrical model, we include them *only in the edge region* ($r > r_*$) with uniform *effective* concentration parameter f_0, representing a sort of radial and poloidal average of their true concentration. As far as Rad_0 is concerned, we consider atomic line emission, just to have a correct order of magnitude (see estimate in figure A1 of appendix A): other loss mechanisms are included by means of f_0.

Though $r_* \approx a$, we have to distinguish the temperature derivatives at $r = a$ and $r = r_*$. In fact, according to (1) a finite variation of T' occurs across $[r_*,\ a]$, due to the peaking of $\mathfrak{R}$, there produced by the light impurities and neutrals emission, and the ensuing large value of T''. Consequently, a Taylor expansion of the function $T(r)$ within $[r_*,\ a]$ must retain also the second-order derivative term. It is possible to show that, under the reasonable assumption $[\mathfrak{R}(a) - \mathfrak{R}(r_*)]/[\mathfrak{R}(a) + \mathfrak{R}(r_*)] \ll 1$, the approximate relation $T(r_*) \approx X(r_* - a)$ holds, with $X = [T'(a) + T'(r_*)]/2$. See appendix D for the details. Note that $X < 0$ for consistency of this approximation.

We then take radial integrals of equation (1). Thanks to few natural approximations described below, the integral $\int_0^a dr\, r\, \mathfrak{R}$ can be expressed by two densities n_*, n_{bulk}, *representative* of edge and bulk respectively, factoring temperature integrals of the radiation rate coefficients in these two regions:

$$3) \quad \int_0^a dr\, r\, \mathfrak{R} \cong \frac{a^2}{2} n_{bulk}^2 \mathrm{H}_{bulk} - \frac{a}{X}\, n_*^2\, \mathrm{G}_*; \qquad \mathrm{H}_{bulk} = \frac{\int_{T_*}^{T_0} Rad_i dT + \left(Z_{eff} - Z_i\right) \int_{T_*}^{T_0} F\, dT}{T_0 - T_*};$$

$$T_0 = T(0); \;\; ; \;\; \mathrm{G}_* = f_0 \int_0^{T_*} Rad_0\, dT + \left(Z_{eff} - Z_i\right) \int_0^{T_*} F\, dT$$

The approximate equation (3) derives from splitting the above integral into bulk and edge contributions, and replacing the radiation rate coefficient by their temperature averages in these two regions, H_{bulk} and G_*/T_* respectively: $\int_0^a dr\, r\, \mathfrak{R} \cong \int_0^{r_*} dr\, r\, \mathfrak{R} + \int_{r_*}^a dr\, r\, \mathfrak{R} \approx \left(\int_0^{r_*} dr\, r\, n_e^2\right) H_{bulk} + \left(\int_{r_*}^a dr\, r\, n_e^2\right) G_*/T_* \approx \frac{a^2}{2} n_{bulk}^2 \mathrm{H}_{bulk} + a(a - r_*) n_*^2\, G_*/T_*$. Use is made of $r_* \approx a$. Then, the radial width of the edge radiative region is expressed through the temperature gradient X, by exploiting the above-mentioned relation $(a - r_*) \approx -T_*/X$.

The half-sum of the integrals of (1) over $[0, a]$ and $[0, r_*]$, yields a second-order algebraic equation for X, taking into account the complete integral (3), the bulk contribution $\int_0^{r*} dr\, r\, \mathfrak{R} \cong \frac{a^2}{2} n_{bulk}^2 \mathrm{H}_{bulk}$, the volume-average heating power density $\langle \wp \rangle = 2 \int_0^a r\, \wp\, dr/a^2$, and the approximation $r_* \approx a$, which applies to everything, but T':

4) $2\, K_* X^2 + a[\langle \wp \rangle - n_{bulk}^2 H_{bulk}] X + n_*^2 G_* = 0.$

Here $K_* = K(r_*) \approx K(a)$. The discriminant is positive or zero, and there are real-valued negative solutions for X, when

5) $a[\langle \wp \rangle - n_{bulk}^2 H_{bulk}] \geq (8 K_* G_*)^{\frac{1}{2}}\, n_*.$

This condition represents a DL, as we will see soon. First, we note that $T'(a) = 0$ when the discriminant (5) is satisfied as equality, namely at the DL: in this somewhat idealized model the DL corresponds to the condition of vanishing heat flux at the edge, implying the equality of total heating and radiated powers. Nonetheless, the analysis of the explicit numerical solutions of the temperature profile from the full model equations, relaxes appreciably this condition (see section 3 of [9]).

We now explicit the DL embedded in (5) by introducing the profile factor $\delta_n = n_{bulk}/n_*$, and the two densities $n_1 = a\langle \wp \rangle/(8 K_* G_*)^{\frac{1}{2}}$, $n_2 = (\langle \wp \rangle / H_{bulk})^{1/2}$, with obvious meanings from (5): n_1 is the DL for n_* neglecting bulk radiation ($H_{bulk} = 0$; the approximation adopted in [9]); n_2 is the DL for n_{bulk} neglecting edge radiation ($G_* = 0$). After little algebra, the DL condition can be cast into the two following equivalent forms

6) $n_* \leq n_1 \times \Theta(\iota), \quad n_{bulk} \leq n_1 \times \Theta(\iota) \times \delta_n; \qquad \Theta(\iota) = \left[(1 + 2\iota)^{\frac{1}{2}} - 1\right]/\iota, \quad \iota = 2 \delta_n^2 n_1^2 / n_2^2$

The function Θ weighs the contributions of edge and bulk radiations, and it is the first improvement with respect to [9]. When edge radiation is dominant, then $\iota \ll 1$, $\Theta \approx 1$, and $n_* \approx n_1$:

experimentally, this corresponds to a negligible content of heavy impurities. If bulk radiation is dominant, then $\iota \gg 1$, $\Theta \approx (2/\iota)^{1/2}$, and $n_{bulk} \approx n_2$: experimentally, this occurs for a significant contamination by heavy impurities, an unwanted condition.

2.1 General expressions for n_1, n_2.

We now further develop (6), by providing more explicit expressions for n_1 and n_2.
It is convenient writing

7) $n_2(10^{20}m^{-3}) = \left[P(MW)/\left(V\hat{H}_{bulk}\right)\right]^{1/2}; \;\; \hat{H}_{bulk} = 10^{34} \times H_{bulk}$

with $V = 2\pi^2 R_0 a^2$ the plasma volume.
In order to compute n_1, we express the edge conductivity K_* in terms of τ_E and a suitable profile factor. The use of $\tau_E$is the second useful improvement of this paper with respect to [9]. We start from the *operative definition* of τ_E in stationary conditions [11]:

8) $\tau_E = 1.6 \times 10^{-16} \times 3V\langle n_e T\rangle/P = 4.8 \times 10^{-16} V\, \delta_n\, \delta_{nT}\, n_* T_0/P; \qquad \delta_{nT} = \langle n_e/n_{bulk} \times T/T_0\rangle$

Note that δ_{nT} is a pressure profile factor. The approximation of taking same temperature for electrons and main ions in (8) has little impact due to the weak dependence of the final DL scaling laws on τ_E, as we shall see. This definition is combined with an equation for T_0 obtained from (1) integrated twice, first over $[0, r]$, then over $[0, a]$ after a division by r. Under DL conditions $\int_0^a dr\, r\, (\wp - \mathfrak{R}) = 0$, we factor the total heating power (equal to the total radiated power), with radial profiles encapsulated within the integral $\mathfrak{I}_p$:

9) $K_* T_0 = \frac{P}{4\pi^2 R_0}\mathfrak{I}_p; \qquad \mathfrak{I}_p = \int_0^a dr \frac{1}{r\,\hat{K}}\left(\frac{\int_0^r dy\, y\, \hat{\wp}}{\int_0^a dy\, y\, \hat{\wp}} - \frac{\int_0^r dy\, y\, \hat{\mathfrak{R}}}{\int_0^a dy\, y\, \hat{\mathfrak{R}}}\right);$

$$\hat{K} = K/K_*\,; \quad \hat{\wp} = \wp/\wp(0)\,; \quad \hat{\mathfrak{R}} = \mathfrak{R}/\mathfrak{R}(r_*)$$

Note that $\mathfrak{I}_p$ is dimensionless. Combination of (8), (9) yields

10) $K_* = 2.4 \times 10^{-16}\, a^2 n_*/\tau_E\, \Psi_p, \qquad \Psi_p = \delta_n \delta_{nT} \mathfrak{I}_p,$

with Ψ_p a further profile factor. If $\widehat{\mathfrak{R}}$ peaks in the peripheral region, as in a plasma polluted by light impurities, the radiation term should be a minor contribution in $\mathfrak{I}_p$ (ignored in [9]).

By replacing K_* with (10) in the definition of n_1, and exploiting the first of the DL relation (6), namely $(n_*)_{DL} = n_1 \times \Theta(\iota)$, one gets

$$11)\quad n_1(10^{20}m^{-3}) = 0.51 \times \left[\Psi_p\ \Theta(\iota)\right]^{-1/3} \left[\frac{P(MW)}{a^2R_0}\right]^{\frac{2}{3}} \left(\frac{\tau_E}{\hat{G}_*}\right)^{\frac{1}{3}}; \qquad\qquad \hat{G}_* = 10^{35} \times G_*$$

The numerical pre-factor and the first parenthesis are dimensionless, whereas the last two parenthesis carry physical dimensions ($\hat{G}_*$ has units of $m^3W\ keV$). Note that (11) is an implicit relation (since $\iota = 2\delta_n^2 n_1^2/n_2^2$) to be solved iteratively, after computing n_2. Factor Ψ_p, like the similar quantity Ψ defined below equation (17), mainly depends on the thermal conductivity radial profile. Both Ψ_p and Ψ are estimated by numerical solutions of equation (1) written for normalized quantities, in appendix B. It turns out that they can be approximated by simple power-law expressions of the profile factors δ_n, $\delta_T = \langle T/T(0)\rangle$, $\delta_{Rad} = \int_0^1 dxx\mathfrak{R}/\int_{x*}^1 dxx\mathfrak{R}$, referring to density, temperature, and radiation respectively. This is a convenient representation, since δ_n and δ_T are generally obtained from measurements, whereas δ_{Rad} can be estimated by means of equation (3): $\delta_{Rad} = 1 + [T_*a/2(a - r_*)]\delta_n^2\, H_{bulk}/G_*$.

Expression (11) can be applied to any magnetic configuration, by specializing τ_E and Ψ_p. We now provide two examples: the stellarator and the L-mode tokamak. Moreover, we also derive a Greenwald-like expression from (11), having a tenuous dependence on τ_E.

2.2 n_1 for the Stellarator

Replacing in (11) the International Stellarator scaling 95, $\tau_E^{ISS95}(s) = 0.079 \times B_\phi^{0.83}\ P(MW)^{-0.59}\ n_{bulk}(10^{19}m^{-3})^{0.51}\ a^{2.21}\ R_0^{0.65}\ \iota_{2/3}^{0.4}$, including the rotational transform $\iota_{2/3}$ at $r = 2/3\, a$, a Sudo-like scaling is obtained:

$$12)\quad n_1(10^{20}m^{-3}) \cong 0.257 \times P(MW)^{0.57}\ B_\phi^{0.33}\ R_0^{-0.54}\ a^{-0.72}\ \iota_{2/3}^{0.16}\ \left[\hat{G}_*\ \Psi_p\ \right]^{-0.4}[\delta_n/\Theta(i)]^{0.2}$$

With a non-monotonic fixed parabolic profile for the effective thermal diffusivity ($= K/n_e$), approximating LHD experimental estimates [12], the analysis discussed in appendix B provides the approximation $\Psi_p^{-0.4} \approx 3.62 \times \delta_T^{0.544}\ \delta_n^{-0.396}\ \delta_{Rad}^{0.375}$ (Eq. B6). Then, it is possible to show that (12) is almost equivalent to the DL scaling laws derived in [9] for the stellarator case (equation (26) of that paper) in the pure edge radiation limit ($n_* = n_1$). This model has been taken into consideration for interpreting high-density experiments in Wendelstein 7-X [13]. In particular, a relation featuring the same power and impurity concentration dependences as (12) (the latter is encapsulated within $\hat{G}_*$) well describes DL in that machine [14].

2.3 n_1 for the L-mode tokamak

Setting in (11) the ITER89-P scaling law, including the atomic mass A and the elongation κ, $\tau_E^{ITER89-P}(s) = 0.048 \times I_p(MA)^{0.85}\, B_\phi^{0.2}\, P(MW)^{-0.5}\, n_{bulk}(10^{20}m^{-3})^{0.1}\, R_0^{1.5}(a/R_0)^{0.3}\,(A\,\kappa)^{0.5}$, one gets:

$$13) \quad n_1(10^{20}m^{-3}) \cong 0.175 \times P(MW)^{0.517}\, I_p(MA)^{0.293}\, B_\phi^{0.069}\, R_0^{-0.276}\, a^{-1.275}\left[\hat{G}_*\, \Psi_p\, \Theta(\iota)\right]^{-0.345}(A\,\kappa)^{0.173}$$

With respect to (11), the power dependence reduces from $P^{2/3}$ to $\sim P^{0.5}$, and the current dependence $\sim I_p^{0.3}$ appears. Note that (13) can be interpreted as a Sudo-like scaling similar to (12), with the toroidal field replaced by the plasma current. By taking a radially increasing thermal diffusivity, suggested by experimental transport analysis in L mode [15], appendix B provides the approximation $\Psi_p^{-0.345} \approx 2.83 \times \delta_T^{0.529}\, \delta_n^{-0.321} \delta_{Rad}^{0.269}$ (Eq. B5). Scaling (13) has not been considered in the previous analysis [9].

2.4 A current dependent form of n_1

For the tokamak and the RFP, the latter considered as purely ohmic, it is possible deriving a further expression of n_1, having a net dependence on I_p, without making any assumption on τ_E. As already shown in [9], this is carried out by including the on-axis Ohm's law with Spitzer resistivity η (neoclassical effects vanish at r=0). Assuming stationary conditions, the toroidal loop voltage $V_\phi = 2\pi R_0 E_\phi$ is radially constant, and we write

$$14) \quad V_\phi = 2\pi\, R_0\, \eta(0)\, J_\phi(0)\, \xi(0)\, C(0) = 0.2 \times \pi\, R_0\, \eta_1\, \zeta\, Z_{eff} T_0^{-\frac{3}{2}}\; J_\phi(0)/\langle J_\phi \rangle\; n_G\;\; \xi(0)\, C(0);$$

$$\zeta = 0.58 + 0.74/\left(0.76 + Z_{eff}\right)$$

Several quantities are defined: $\eta_1 = 0.0165 \times ln\Lambda \left(\Omega\, m\, keV^{3/2}\right)$ [16], with $ln\Lambda$ the Coulomb logarithm; $C(r) = E_\phi J_\phi/(\eta\, J^2)$ is the RFP anomaly function, modelling the effect of the dynamo process [17] ($C = 1$ for the tokamak); $\xi(r) = J_\Omega / J \leq 1$ is the current-drive function related to the additional heating, with $J,\ J_\Omega$ the current density magnitude, total and ohmic respectively ($\xi = 1$ for the ohmic tokamak and the RFP). In a more general sense, $\xi(0)$ could also include an anomaly factor for the tokamak: in this case it would not be constrained to be ≤ 1 ($\xi = 1$ for the RFP, anyway). In the second equality of (14) we replace $J_\phi(0) \rightarrow 10^6 \times J_\phi(0)/\langle J_\phi \rangle \times n_G$, being $n_G = 10^{-6} \times \langle J_\phi \rangle = I_P(MA)/(\pi a^2)$, and $J_\phi(0)/\langle J_\phi \rangle$ a profile factor for the current, to be included in a more global shape factor, as we will see later. Though we use the same definition of the Greenwald empirical parameter, n_G has not the dimensions of a density, but of *a current density*.

The simple relation $P = 4\pi^2 R_0 \int_0^a \eta J^2\ r\, dr = 4\pi^2 R_0 \int_0^a E_\phi J_\phi\ r\, dr\ =\ V_\phi\ I_p$ holds in the ohmic tokamak: in such a case, it is natural making use of (14) to develop further the power term of (11). However, this relation does not apply neither in the additionally heated tokamak, obviously, nor in the RFP, due to the anomaly function. The idea underlying the following derivation is to factor the term $V_\phi\ I_p$ within *P in all cases,* leaving to further terms the task of discriminating between the different configurations. In particular, for the tokamak we consider the identity

$$15)\ \ P = I_p\, V_\phi / \xi(0)\ \times \Pi_{tok}; \qquad\qquad \Pi_{tok} = \xi(0) P / \left(V_\phi I_p\right)$$

where Π_{tok} can be interpreted as the power enhancement with respect to the pure ohmic heating (without anomaly, $\xi(0) = 1$, hence $\Pi_{tok} = 1$, for the ohmic tokamak). For the RFP, starting from $P/(4\pi^2 R_0) = \int_0^a \eta J^2\ r\, dr = \int_0^a E_\phi J_\phi / C\ \ r\, dr$, we derive the similar expression

$$16)\ \ P = I_p\, V_\phi / C(0)\ \times \Pi_{RFP}\,; \qquad\qquad \Pi_{RFP} = \frac{1}{a\, B_\theta(a)} \int_0^a \frac{d}{dr}(r B_\theta)\ \hat{C}^{-1}\, dr$$

with Π_{RFP} a dimensionless profile factor for $\hat{C} = C/C(0)$. Leaving $\Pi_{tok}, \Pi_{RFP}, \xi(0), C(0)$ unaltered, expressions (15), (16) are then modified by equation (14) for V_ϕ, in combination with (9) for T_0, (10) for K_*, and the DL equality (6) for n_*. Afterwards, they replace the term $P^{2/3}$ in (11). As shown in more detail in appendix C, scaling (11) turns into:

$$17)\qquad n_1(10^{20} m^{-3}) = \Pi^{\frac{4}{9}} \times n_{\mathrm{Oh}}; \qquad n_{\mathrm{Oh}}(10^{20} m^{-3}) = 0.425 \times \left[\left(\zeta\, Z_{eff}\right)^{\frac{4}{9}} \Psi^{\frac{10}{9}}\, \Theta(\iota)^{\frac{1}{9}}\right] \times \left(\eta_1^{\frac{4}{9}}\, \hat{G}_*^{-\frac{5}{9}}\, \tau_E^{-\frac{1}{9}}\, n_G^{\frac{8}{9}}\right); \qquad \Pi \in \left\{\Pi_{tok} = \xi(0) P / \left(V_\phi I_p\right),\ \Pi_{RFP}\right\}; \quad \Psi = \left[J_\phi(0)/\langle J_\phi \rangle\right]^{\frac{2}{5}} \mathfrak{I}_p^{-\frac{3}{5}}\, \Psi_p^{\frac{1}{10}}$$

Note that the dependence on $C(0)$ eventually disappears, and that Π has different meanings for tokamak and RFP. The density n_{Oh} is n_1 for the ohmic tokamak (with no anomaly): in its definition, the numerical pre-factor and the first parenthesis are dimensionless, whereas the last parenthesis carries the density dimension. Quantity Ψ is a further profile term, including a shape factor for the toroidal current density. The numerical analysis described in Appendix B justifies the approximation $\Psi \approx 4.43 \times \delta_T^{0.825}\ \delta_n^{0.166}\delta_{Rad}^{0.387}$ for the L-mode tokamak (Eq. B4), and estimates a similar value in the RFP case (for typical profiles of RFX-mod): $\Pi_{RFP}^{4/9} \times \Psi^{10/9} \sim 3.7$.

While scaling (11) agrees with the insight of a DL ruled by the competition between input power, energy transport and radiation losses, scaling (17) is far less intuitive. In particular, the final appearance of a *net current dependence* ($I_p^{8/9}$ in ohmic devices, $I_p^{4/9}$ for the auxiliary heated tokamak) is the result of the combination of all the equations mentioned above.

Equation (17) is almost equivalent to scaling (13) of reference [9], given the follow correspondence between the quantities here defined and those of that paper: $\hat{G}_* \to \tilde{R} \times f_*(\%)$, $\Pi_{RFP} \to \psi(a)$, $\Im_p \times \left(J_\phi(0)/\langle J_\phi \rangle\right)^{-1} \to \widehat{\Im} \times \psi(a)^{-1}$. Nonetheless, the present scaling arranges slightly better the factors (in particular the explicit dependence $(R_0/a)^{1/5} \times B_\phi(0)^{-1/5}$ in equation (13) of [9] is assimilated in the other terms) and replaces K_* with τ_E, thus reducing the dependence on n_G from exactly linear to the power 8/9.

For ohmic devices, either tokamak ($P = V_\phi I_p$) or RFP, scaling (17) features a Greenwald-like term ($n_G^{8/9}$), and shows a *negligible dependence on energy confinement* ($\tau_E^{-1/9}$). This fact, alongside the similarity of $\Pi^{4/9} \times \Psi^{10/9}$ in the two cases, brings the first explanation of the experimental observation of an almost identical DL in these widely different configurations (as far as the RFP DL is concerned, we mention the RFX-mod experiments [18, 19], which are reproduced quite well by the model, as shown in [9]).

For the additionally heated tokamak, a further implicit dependence on transport is implied by the presence of V_ϕ within Π_{tok}. In this case, note also the overall dependence on power and current, $P^{4/9}\ I_p^{4/9}$, similar to that of (13). This near coincidence is not obvious, though both scalings (13) and (17) are derived from (11). In fact, the former stems from the specific power and current dependences ${I_p}^{0.85}\ P^{-0.5}$ of the ITER89-P scaling law, whereas the latter does not rely on any assumption on τ_E. Might then be possible that the equations linking (11) to (17) imply current and power dependencies for τ_E similar to those of $\tau_E^{ITER89-P}$? This is indeed the case, as simply verified by matching (11) and (17). This leads to the important corollary that an effective expression for τ_E, *valid in or close to DL conditions*, may be written. Letting $ln\Lambda \to 15$, $\zeta \to 1$, for the sake of simplicity, one gets

$$18)\ \ \tau_{E,DL}(s) = 0.0165 \times Z_{eff}\ \hat{G}_*^{-\frac{1}{2}}\, \Pi\, P(MW)^{-3/2}\ I_p(MA)^2\ R_0^{3/2} a^{-1}\, \Psi^{5/2}\ \Psi_p^{3/4}\Theta.$$

For the tokamak ($\Pi = \Pi_{tok}$), the scaling becomes

$$19)\ \ \tau_{E,DL}^{tok}(s) = 0.0165 \times Z_{eff}\ \hat{G}_*^{-\frac{1}{2}}\, \xi(0)\ V_\phi^{-1}\ P(MW)^{-\frac{1}{2}}\ I_p(MA)\ \ R_0^{3/2} a^{-1}\ \ \Psi_{tok}^{5/2}\Psi_p^{3/4}\Theta$$

Note that, the power and current exponents of (19) are almost identical to those of the ITER89-P scaling law. Since no specific hypothesis on the underlying transport mechanism is made, they are understood as global constraints set by the fluid equations used to go from (11) to (17). The good confinement property of the tokamak is quantified by the typical low values of V_ϕ required to sustain the discharge: $\xi(0)/V_\phi \sim o(1)\ Volt^{-1}$. We cannot say whether (19) might provide some insight in the power and current dependences of the ITER89-P scaling law, since it depends on the DL relation $n_* = n_1 \times \Theta(\iota)$, whereas ITER89-P has been obtained far from this condition. We leave the above discussion as suggestive of the possibility that also MHD, besides micro-turbulence, could be at the origin of the power and current dependences found in the empirical scaling laws of the energy confinement time.

3. JET L-mode experiments

This DL model is applied to a database of L-mode disrupted JET discharges. They terminated during a density ramp-up, which should make it likely that we are dealing with DL disruptions. We consider 21 discharges with Carbon (C) wall (shots 43161, 43547, 45479, 50427, 52194, 52318, 52436, 52442, 52651, 52690, 53138, 53140, 54000, 55288, 55539, 55541, 55543, 56117, 59648, 75673, 76285) and 5 discharges with Beryllium-Tungsten wall (Be-W) (shots 81491, 82342, 86953, 86956, 87494). They are all in Deuterium (D), but for shot 54000, which is in Helium (He), and 52651, which disrupted after a Neon (Ne) seeding.

3.1 Model parameters setting

Several experimental quantities have to be plugged in the model, besides the straightforward $R_0 = 2.98m,\ a = 0.95m, A, \kappa, I_p$. For both density and temperature, Thomson scattering provides the on-axis values, n_{e0}, T_0, and the volume-average values $\langle n_e\rangle, \langle T_e\rangle$, in the whole database. The density profiles are generally weakly peaked, particularly when density increases, since $n_{e0}/\langle n_e\rangle < 1.5$. While the identification $n_{bulk} \to \langle n_e\rangle$ is rather straightforward, no reliable edge density measurements are available on the complete database. Therefore, fixing the reasonable value $r_* = 0.9a$, we estimate $n_*^2 = \int_{r_*}^{a} dr\, r\, n_e^2/[a(a-r_*)]$, with the profile $n_e(x) = n_{e0}(1-x^2)^{\nu}$, being $x = r/a$ and $\nu = n_{e0}/\langle n_e\rangle - 1$. The temperature $T_* = T(r_*)$ is computed by assuming the same kind of profile, $T_e(x) = T_0(1-x^2)^{\gamma}$, with $\gamma = T_0/\langle T_e\rangle - 1$: typically, $T_* \sim 0.1 \div 0.4 keV$. The high-resolution, edge Thomson scattering signals are available only in six shots of this database: there, our estimates of edge density and temperature are compatible with those measurements.

As far as heating power P is concerned, the ohmic input, typically below 2MW, is evaluated by V_{ϕ} and I_p. Few of the present discharges include ICRH heating, but the majority of them features NBI heating. Due to several loss mechanisms, only a fraction of the NBI injected power contributes to P. The best we can do to quantify losses is adding the shine-through power, available as a pulse-file signal, to the fraction of power lost by charge-exchange and unconfined orbits, estimated by $0.01 \times exp\left[3.35 - 0.667/I_p(MA) - 0.2 \times \langle n_e\rangle(10^{19}m^{-3})\right]$ [20]. The shine-through turns out to be a minor effect, and it is not considered on the whole database. The total losses are rather small, less than 20% when density increases. Figure 1 displays the ratio between the total and ohmic components of P, alongside the volume average Z_{eff}, which is available from visible bremsstrahlung.

The density, temperature, and radiation shape factors, in terms of which we approximate Ψ_p, Ψ, are estimated as follows: $\delta_n \approx \langle n_e\rangle/n_*$ is provided by the above reconstruction; $\delta_T = \langle T_e\rangle/T_0$ is given by the Thomson scattering data; δ_{Rad} is computed for $r_* = 0.9a$, following the definition given at the end of paragraph 2.1. Note that, δ_n enters also in the function Θ. Finally, factor $\xi(0)$ within Π_{tok} is estimated by inversion of equation (14), taking the standard toroidal current density model for tokamak, $J_{\phi} = I_p/(\pi a^2) \times q(a)/q(0) \times (1-x^2)^{q(a)/q(0)-1}$ [16], and $q(0)$ from equilibrium reconstruction. We generally obtain $\xi(0) \gtrsim 1$, which supports the presence of an anomaly effect in this parameter.

Several quantities are needed to estimate the radiation terms $\widehat{H}_{bulk}$, $\widehat{G}_*$. First, T_0, T_*, which are provided by Thomson scattering as discussed above. Then, the standard functions $Z_j(T), Rad_j(T), Rad_i(T), Rad_0(T)$ are taken from the database [21]. For W we make also use of [22]. More details are given in appendix A. Finally, the parameters $\hat{f}_j$, f_0, the former entering in the definition (2) of the average radiation rate coefficient F, are more difficult to assess, even though spectroscopic measurements guide the choice. Let's first consider the deuterium discharges with C wall, forming the major part of the present database. In this kind of shots, neutral deuterium (D_0) and C impurity are the main contributors to radiation in the SOL region [23]. Therefore, we take D_0, C, and a smaller fraction of Oxygen (O) [24], as emitting species. Due to the similarity between Rad_O

and Rad_C, model output turns out to be almost independent on their relative concentration $\hat{f}_O = f_O/f_C$. Results will be displayed for $\hat{f}_O = 0.1$. The D_0 effective concentration parameter f_0 is estimated taking as reference the ratio, here named Q_*, between the powers radiated by neutrals and impurities in the peripheral region. According to the experimental observation [23], we should take $Q_* \sim 1$ in C wall discharges. More precisely, we fix $Q_* = 2$, on the basis of the EDGE2D/EIRENE simulations discussed in figure 10 of [23]. We choose f_0 in order to verify this requirement on average, by setting $f_0 = Q_* \overline{\left(Z_{eff} - Z_\iota\right) \int_0^{T*} FdT / \int_0^{T*} Rad_0 dT}$, with the bar denoting the time average over a wide interval ($\sim 10s$). Between shots, f_0 varies in the range $f_0(\%) \sim 0.1 \div 0.6$. The same criterion is used to set $f_0$in the He discharge 54000. The Ne seeded shot 52651 is excluded from this procedure, and it will be discussed later on. As far as the Be-W wall shots are concerned we limit the impurity content to Be and a small fraction of C (we take $\hat{f}_C = f_C/f_{Be} = 0.1$ [24]). Typically, negligible W content ($f_W \sim 1 \div 5 \times 10^{-6}$) is reported [23]: only in shot 87494 we need including W to match the experimental DL. Neutral deuterium is the main contributor to SOL radiation in these kind of discharges [23], due to the low radiation capability of Be. In particular, the above-mentioned EDGE2D/EIRENE simulations suggest $Q_* \sim 5$. However, due to the large Q_* factoring a $Z_{eff} - Z_i$ sometimes getting close to 0, the function $Q_* \left(Z_{eff} - Z_i\right) \int_0^{T*} FdT / \int_0^{T*} Rad_0 dT$ is too irregular in time to be considered as meaningful. Hence, in these discharges we set f_0 equal to the ensemble average previously obtained in the whole C wall subset for $Q_* = 2$: $f_0(\%) \sim 0.3$. The same value is fixed for the Ne seeded shot 52651. A sensitivity study of the model output from the choice of Q_* is provided in a dedicated paragraph.

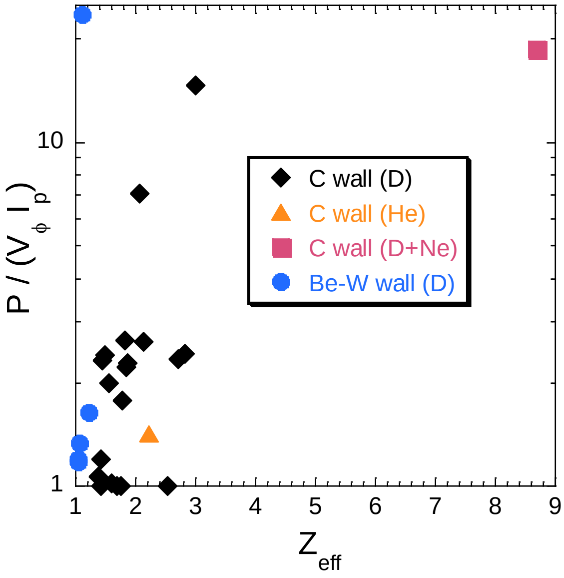

Fig. 1. Ratio between total and ohmic power input vs Z_{eff} for each discharges of the database. The power ratio is time averaged over a significant interval, whereas the Z_{eff} values represent the final 0.2s before the disruption. Note that y-axis is in log-scale.

3.2 Density limit analysis

In the following figures we display *the full time trace up to the disruption* of several quantities, excluding only the initial start-up phase, for each discharge of the database. Visible symbols are also superimposed to mark the disruption events: they represent the average of the considered quantities taken in a time interval of 0.2s before the termination. Figure 2 provides an assessment of the Greenwald DL $\langle n_e\rangle(10^{20}m^{-3}) = n_G$. The result is rather negative: not only the majority of the disruptions occurs at densities significantly smaller than n_G, but, furthermore, the dispersion of the disrupted points at any given n_G is very large. Therefore, the pure n_G criterion is not sufficient for a shot-by-shot description of the termination events in the present database. Figures 3 and 4 consider two equivalent comparisons with the model, related by a multiplication by δ_n: in the former, the estimated n_* is plotted against the first of (6); in the latter $\langle n_e\rangle$ is plotted against the second of (6). We further diversify them by changing the expression for n_1: equation (17) in figure 3 (the weak factor ${\tau_E}^{1/9}$ is expressed by the ITER89-P scaling); equation (13) in figure 4. The two choices give similar results, in agreement with the fact that scaling laws (13) and (17) are rather close, as far as the dependences on power, current and impurity factor $(\hat{G}_*)$ are concerned. With respect to the pure n_G criterion, they avoid a systematic overestimate, better delimit the density space, and better align the disrupted points. This improvement is quantified by the analysis presented in paragraph 3.3.

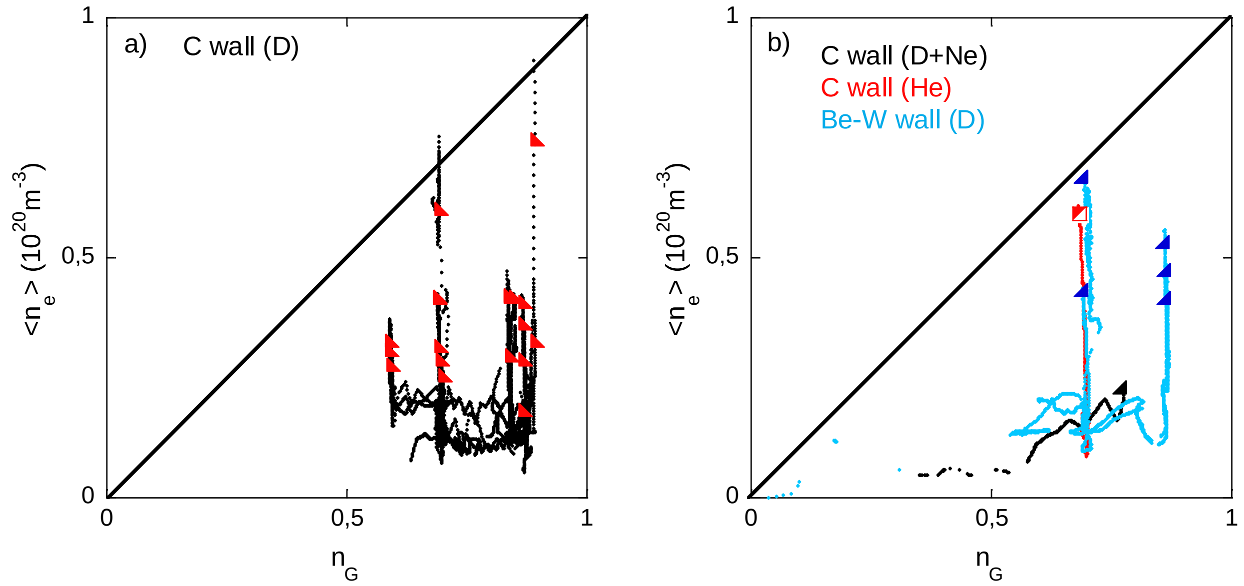

Fig. 2. Volume-average density vs. n_G for the whole database. C wall shots in D are plotted in (a). In plot (b) we display Be-W wall shots (cyan), the C wall shot in He (red) and the C wall shot with Ne puffing (black). The triangles and the square mark the disruptions. The straight black line is the bisector y=x.

In plots 3b and 4b, the termination of shot 87494 is marked with a different symbol (blue circle), since there we need including a small fraction of W for the model to agree with the experiment (or, a significantly larger f_0, option not considered). This is not unreasonable: having this shot by far the highest (NBI) power within the present Be-W database (in figure 1 it is represented by the blue circle in the top left corner), it is possible that a small amount of W, coming from the divertor plates, must be included here. However, the choice of Rad_W turns out to be an issue when the low temperature region needs to be included, as in the present case. Let us consider the two estimates given in [21, 22], and reported in figure A2 of appendix A: the former features a peak at $T \sim 2eV$, orders of magnitude larger than the maximum radiation rate coefficient of any light impurity; the latter, while similar to the previous one for high temperatures, is truncated for $T < 30eV$, where atomic data are considered uncertain. The data of shot 87494 shown in figures 3b, 4b correspond to this second option, with Rad_W *set to zero* for $T < 30eV$, and $\hat{f}_W = f_W/f_{Be} = 0.05$. A sensitivity study of the model dependence on $\hat{f}_W$ is discussed in [25]. A stronger dependence on $\hat{f}_W$ is found when using Rad_W from [21]: agreement between experimental and modelled DL is recovered for values of $\hat{f}_W$ one order of magnitude smaller ($\hat{f}_W \sim 0.003$).

Finally, a brief comment about the trajectory of shot 52651 (C wall, D+Ne) in figures 3b, 4b. In the second half of the discharge, about one second before puffing Ne, a strong NBI heating (about 6MW) is applied, and the points move to the right part of the plot. Then, keeping NBI heating unaltered, Z_{eff} progressively increases (up to 8), bringing back the points to the left. The termination eventually occurs with the trajectory heading towards the expected limit, though not reaching it. The trajectory is much less explicative when the density is plotted against n_G (figure 2b) since the motion is not directed towards the limit, but it is parallel to it.

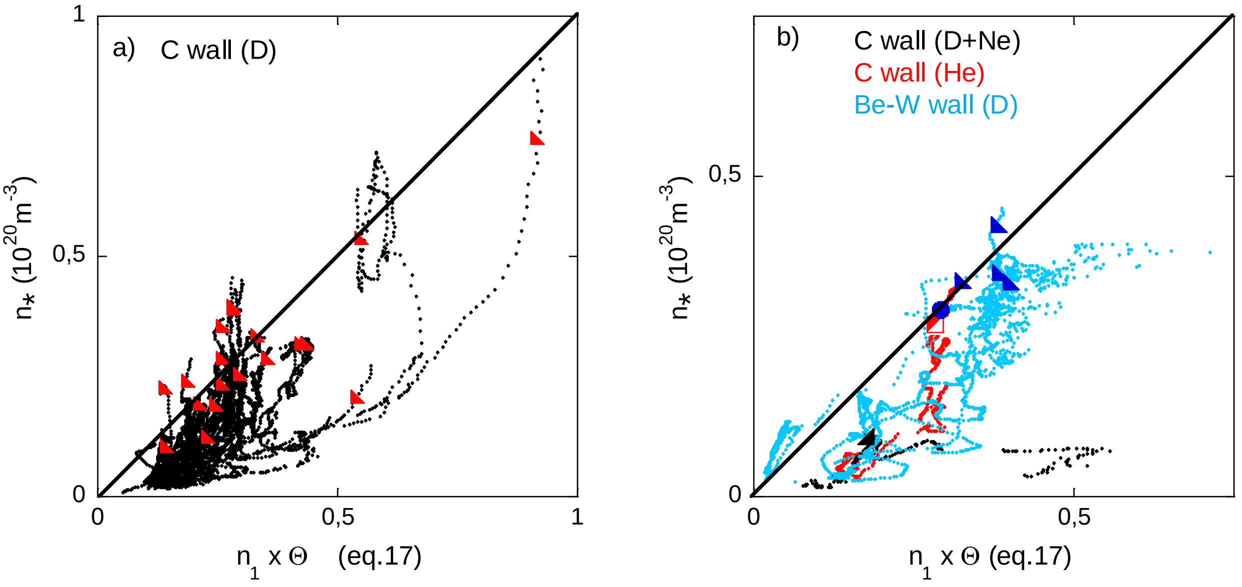

Fig. 3. Estimated experimental edge densities versus modelled edge DL, with n_1 given by (17). Same colour code as figure 2. The blue circle in plot (b) (exactly along the bisector) marks the disruption for shot 87494 where a small W fraction is included in the model.

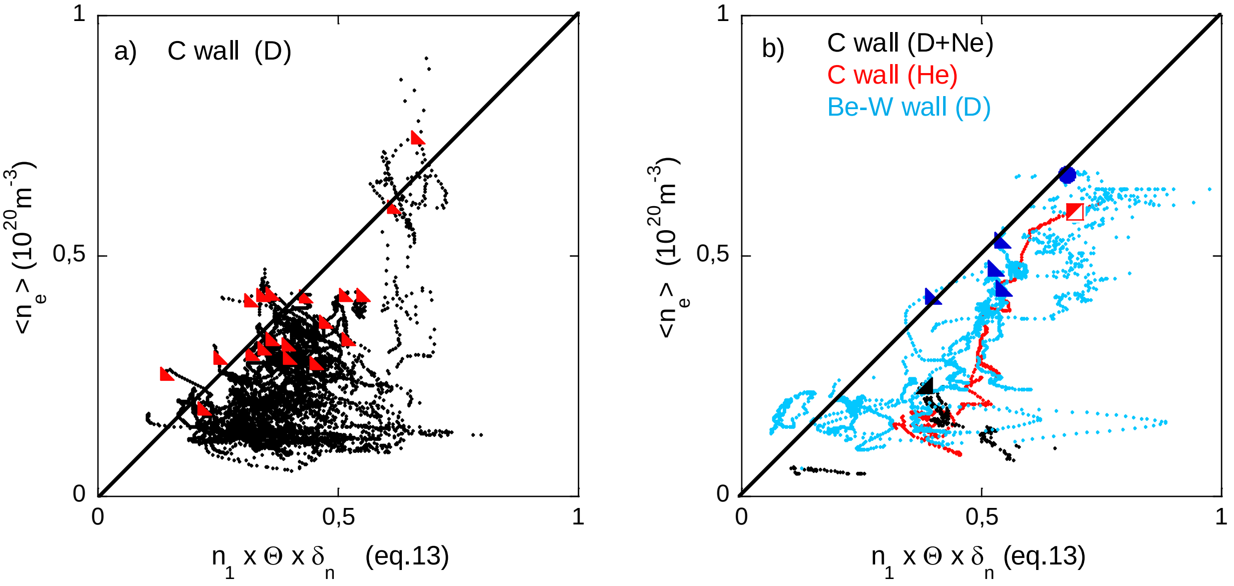

Fig. 4. Volume-average densities versus modelled bulk DL, with n_1 given by (13). Same colour code as figure 2. The blue circle in plot (b) (exactly along the bisector) marks the disruption for shot 87494 where a small W fraction is included in the model.

3.3 Study of the dependence on f_0

A sensitivity study with respect to f_0 is now presented. We recall that f_0 is not the true physical concentration, but an effective parameter. As described in paragraph 3.1, for each discharge of the C wall subset f_0 is estimated through a time-average, by fixing the ratio Q_* between the powers radiated by neutrals and impurities in the peripheral region. Then, the shot-average of the f_0 values so obtained fixes this parameter in the Be-W wall subset. The agreement between experiment and model is assessed for several values of Q_*, as follows. For a given Q_*, referred to the C-wall subset, we consider the experimental n_* and the modelled edge DL, the latter from equations (6), (17) with the computed f_0 as input. These values are taken close to the disruption in the whole database (as the disruption marks of figures 3a, 3b, which refer to $Q_* = 2$), excluding the Ne seeded shot 52651. Then, we take a liner fit of the points, forcing it to pass through the origin: $y = c\,x$. Results are summarized by figure 5, displaying the fit parameters c and χ^2 against the shot-average f_0, for the different values of Q_*. The model dependence on f_0 turns out to be rather weak, considering that this parameter, as well as Q_*, spans two order of magnitude. Take also into account that values outside the range $Q_* = 0.5 \div 5$ are quite unlikely. In any case the model works better than the Greenwald criterion, which is tested by a similar linear fit between $\langle n_e \rangle (10^{20} m^3)$ and n_G at the disruption, whose parameters are reported in the rectangular insertion, with no reference to f_0. In particular note the poor quality of the fit, quantified by a χ^2 significantly larger than any of the value obtained with the model.

Overall, the proposed model is definitely better than the pure n_G criterion, in the considered database. Nonetheless, the unavoidably uncertainties of the emitting species' parameters make hard obtaining more than an assessment of compatibility from the comparison with the experimental data.

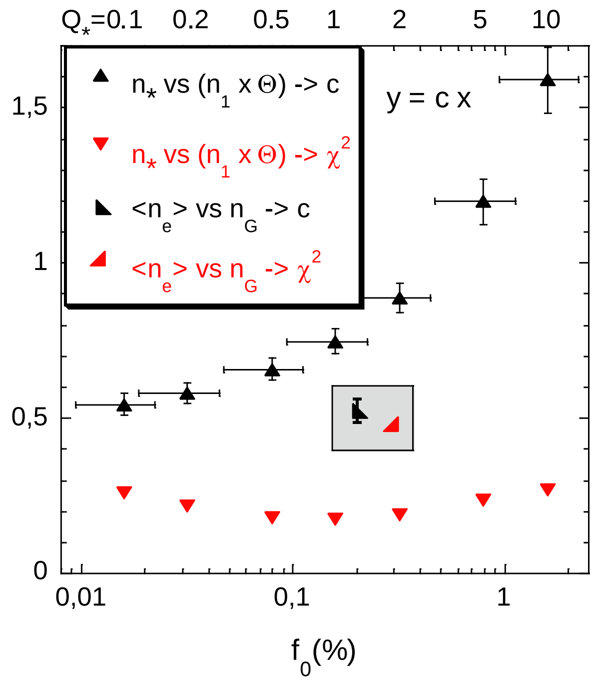

Fig. 5. Parameters of the linear fit $y = c\,x$, applied to the experimental n_* ($\rightarrow y$) and modelled edge DL ($\rightarrow x$), with $n_1$from equation (17), at the disruptions in the whole database, but the Ne seeded shot 52651. For different Q_* (referred to the C-wall subset and reported above the plot), both c, with (vertical) error bar, and χ^2 are displayed against the shot-average of the effective concentration parameter f_0, reported with the

standard deviation (horizontal bar). Note the log-scale for the f_0-axis. The symbols in the rectangular insertion are not referred to any value of f_0, being the parameters of the fit applied to $\langle n_e\rangle(10^{20}m^3)$ $(\rightarrow y)$ and n_G $(\rightarrow x)$ taken at the disruptions.

3.4 Disruptions after NBI switching off

We also consider three further C wall discharges (shots 52440, 53974, 54033), which disrupted shortly after switching off the auxiliary (NBI) heating, while density stays nearly constant. The behaviour can be understood by looking at the time traces of the estimated n_* and of the modelled DL, as plotted in figure 6. Due to the dependence on P, the predicted DL drops at the NBI switching off. Shot 54033 (plot a) is the most significant case, having the largest NBI input: the density stays well below the expected DL for most of the discharges, but suddenly goes above the limit when the latter drops alongside P (time>64s) and a disruption occurs. The same behaviour can be seen in shot 52440 (plot b). In shot 53974 (plot c), though recognizable, it is not so clear, since density stays close to the modelled DL during the NBI phase. These examples provide a clear indication in favour of the DL dependence on P, taking also into account that n_G and Z_{eff}, two further important quantities of the scaling (17), are almost constant in the considered time windows.

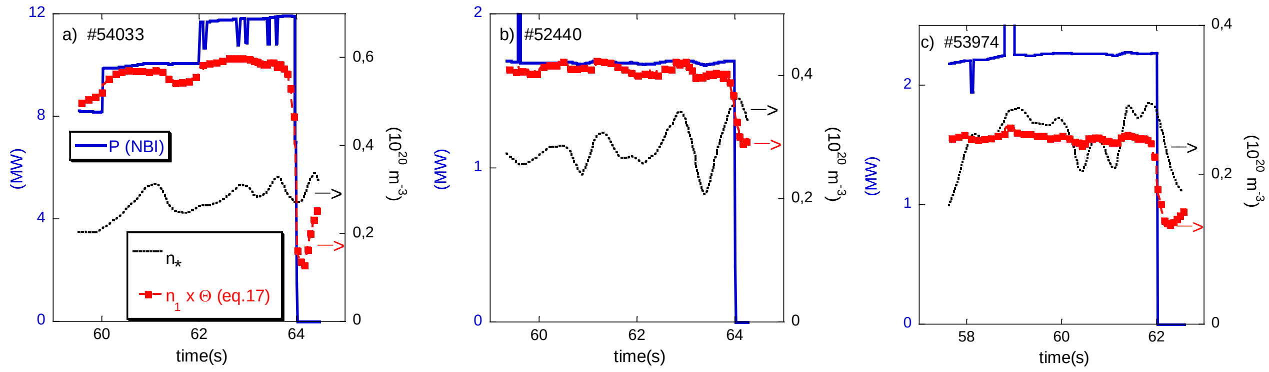

Fig. 6. Several time traces up to the disruption, for three shots: P from NBI (blue, solid line); edge density n_* (black, dotted line); predicted edge DL, $n_1 \times \Theta$, with n_1 from equation (17) (red line with symbols).

4. A reduced scaling of n_{bulk} for the L-mode tokamak

The DL scaling law (6), with any of the expressions for n_1 so far derived, contains several terms not straightforward to determine. First, the edge density n_* and the profile factor $\delta_n = n_{bulk}/n_*$: they require a good reconstruction of the profile in the edge region, but this is not always guaranteed in the experiments. Moreover, there is a certain vagueness in the definition (3) of n_*, though it is clear that it refers to the peripheral region of the plasma. Second, the shape factors Ψ_p, Ψ, which involve integrals: they can be approximated by powers of the profile factors referring to the ‘primary’ quantities, namely temperature, density and radiation, but this nothing more than an estimate (see appendix B). Finally, the current-drive factor $\xi(0)$ in scaling (17): its evaluation by inversion of (14) requires stationary conditions for radial constancy of V_ϕ, which is not always guaranteed, as well as an estimate of the current profile factor $J_\phi(0)/\langle J_\phi \rangle$. As explained in paragraph 3.1, we did our best to evaluate these terms, exploiting all relevant experimental signals available in the JET database. Nonetheless, this procedure might introduce some degree of noise, due to the uncertainties discussed above. Therefore, it is also worth considering a *reduced* scaling law, obtained by replacing the problematic terms with *typical values estimated close to the DL on this database*. The ultimate justification for setting these values is that the ensuing scaling indeed works, as shown later. We start from DL (6) for n_{bulk}, with n_1 given by the tokamak version of (17). Then, we replace $\Psi \rightarrow 2.5$ and $\xi(0)/V_\phi \rightarrow 2\ Volt^{-1}$. Taking into account the inverse dependence of Θ on δ_n, we set $\Theta^{10/9} \times \delta_n \rightarrow 1$: this is justified for *weakly/mildly peaked* density profiles, as those of the database. In addition, we replace $ln\Lambda \rightarrow 15$, $\zeta \rightarrow 1$, and $\tau_E(s)^{-1/9} \rightarrow 1$. We also identify $\int_0^{T_*} F\, dT \rightarrow 4 \times 10^{-35}\ (m^3\ W\ keV)$, which is a typical value obtained for light impurities by taking $T_* > 50eV$ with the radiation rate coefficients shown in figure A1(a) of appendix A. For the sake of simplicity, we set $f_0 \int_0^{T_*} Rad_0\, dT \rightarrow f_0(\%) \times 4 \times 10^{-35}\ (m^3\ W\ keV)$, which corresponds to $T_* \approx 50eV$. Hence, $\hat{G}_* \rightarrow 4 \times \left[f_0(\%) + Z_{eff} - Z_i\right]\ (m^3\ W\ keV)$. Then, a very manageable scaling law for L-mode tokamak DL is derived:

20) $n_{bulk}(10^{20}m^{-3}) = 0.4 \times Z_{eff}^{4/9} \left[f_0(\%) + Z_{eff} - Z_i\right]^{-\frac{5}{9}} \left[P(MW)/I_P(MA)\right]^{\frac{4}{9}} \times n_G^{\frac{8}{9}}$

Note that the numerical pre-factor is not dimensionless in this case. Caveat: this scaling should apply only to weakly/mildly peaked density profiles and for negligible contribution of heavy impurities to radiation.

4.1 Comparison with the JET database

As shown by figure 7, the reduced scaling works at least as well as the complete model (see figures 3, 4) when taking $f_0(\%) = 0.5$, which is a value compatible with the previous estimates. An exception is shot 87494 (blue circle in plot 7b), which needed the inclusion of W when performing the analysis with the complete model: this is indeed a case not well represented by scaling (20).

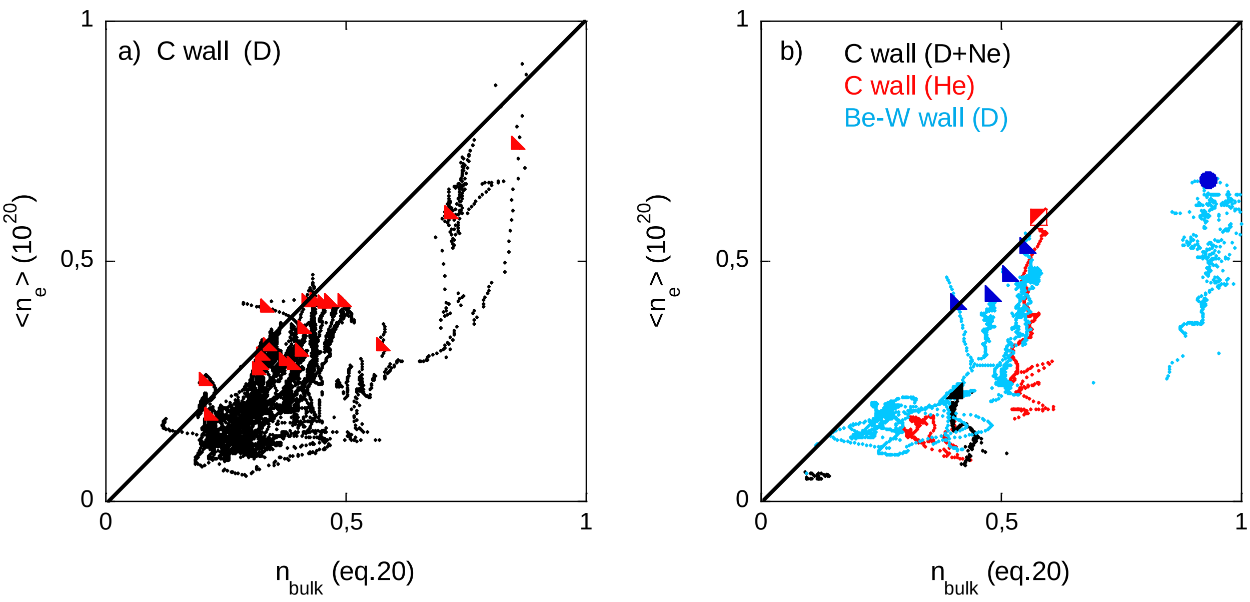

Fig. 7. Volume-average densities versus modelled bulk DL, as given by the reduced scaling law (20) with $f_0(\%) = 0.5$. Same colour and symbol code as figures 3, 4.

4.2 Comparison with published data.

Given the relatively few parameters involved, scaling (20) is well suited to be compared with published data from other L-mode DL experiments. Typically, papers report the maximum line-average densities $\bar{n}_e$, alongside the values of P, I_p, at which they have been attained. Unfortunately, Z_{eff} is not generally given on a shot-by-shot basis, or, at least, it is virtually impossible finding the correspondence with the other quantities of the scaling from the published data. For this reason, we prefer dropping the term $Z_{eff}^{4/9}\left[f_0(\%) + Z_{eff} - Z_i\right]^{-\frac{5}{9}}$ within scaling (20), and comparing the experimental densities with the *residual* DL relation, $n_{bulk}(10^{20}m^{-3}) \sim 0.4 \times \left[P(MW)/I_P(MA)\right]^{\frac{4}{9}} n_G^{\frac{8}{9}}$.

The following experiments are taken into consideration: (I) TEXTOR-94, data from figure 15 (top) of [26] ($I_p = 0.23MA$); (II) JT-60, data from figure 6a of [27] (only the interval $2.8 \div 3.1MA$ is given for I_p; since it is quite narrow, we set its average as current value: $I_p = 2.95MA$); (III) JET in limiter configuration (shot number about 7000, $a = 1.2m$), data from figure 4 of [5]; (IV) ASDEX Upgrade, data from figure 5 (left) of [28] ($I_p = 0.6MA$ for H shots, $I_p = 0.8MA$ for D shots); (V) ASDEX, data from figure 8 of [4] (three values of $q(a)$ are there reported: we get I_p by the relationship $q(a) \propto I_p^{-1.64}$, applying in those particular discharges). First of all, the average densities are compared to n_G in figure 8a: though a global increasing trend is detectable, the data dispersion is too large to regard n_G as the single relevant parameter. Then, scaling $0.4 \times (P/I_P)^{\frac{4}{9}} n_G^{\frac{8}{9}}$ is considered in figure 8b. The comparison with the experimental densities suggests that a factor larger than unity is missing in such residual scaling: this is what the dropped term is expected to be for moderate values of Z_{eff} and f_0. However, even without that important term, this relation aligns the maximum densities much better than the n_G criterion does (we note that the ASDEX Upgrade data in deuterium are slightly off trend).

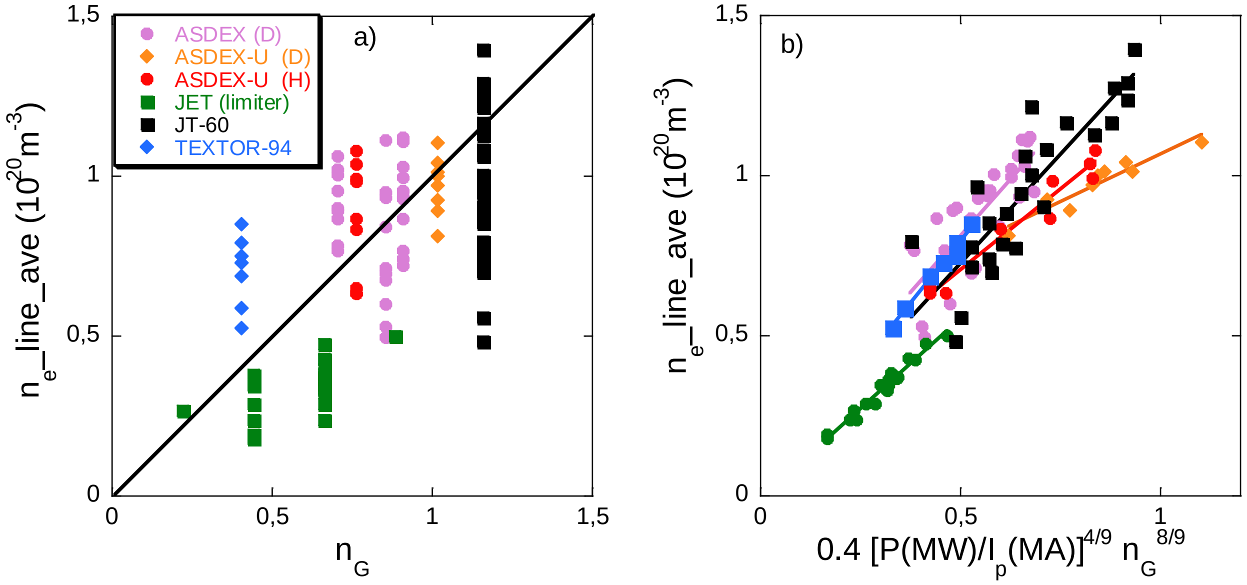

Fig. 8. Maximum line-average densities for different L-mode tokamak experiments, as reported in published papers. The data are plotted vs. n_G in (a), and vs. a sub-scaling derived from (20) in (b). In plot (b), linear interpolations of the data of each experiment are displayed.

5. Comment on the DL power dependence as discussed in references [2] and [29]

As far as the interpretation of the L-mode DL is concerned, the analyses so far discussed leave little doubt about the progress gained passing from the pure n_G criterion to the present model, which includes P as a key parameter. Therefore, it is interesting to understand how the power dependence could be overlooked in the review paper of DL [2]: its paragraph 2.2.4 asserts that this dependence is not significant for the tokamak, or, at least, too weak to be justified by power-balance arguments. As supporting evidence the figure 9a of [29] is reported, referring to DIII-D L-mode experiments. This figure displays the line-average density normalized to I_p as a function of P, at the detachment of the plasma, for some values of I_p and B_ϕ: no dependence on P is visible, and in agreement with this, the scaling $\bar{n}_{det}/I_P \propto P^\beta,\ \beta < 0.15$ is proposed [29]. Taking the data from the original figure 9a of [29] (which benefits of one point more than the copy reported in [2]), we have repeated the analysis, confirming the published result: $\bar{n}_{det}(10^{20}m^{-3}) \approx 0.57 \times I_p(MA)^{1\pm0.06}\ P(MW)^{0.16\pm0.03} B_\phi^{-0.29\pm0.08}$. However, this procedure is subject to two criticisms. The first, most obvious, is that $\bar{n}_{det}$ does not necessarily coincide with the DL: for those experiments this occur only at low/moderate $q(a)$, whereas at higher $q(a)$ the maximum attained density generally exceeds $\bar{n}_{det}$ (see figure 3 of [29]). Unfortunately, the maximum densities corresponding to the points of figure 9a are not reported in that paper. The second, most important, is that the considered database mixes purely ohmic and NBI heated discharges: since in the former subset the two quantities I_p, P are strongly correlated (we find a linear relationship), the previous regression, though mathematically correct, can not provide the *true physical dependences*. In fact, limiting the analysis to the NBI heated subset, where I_p and P might be considered loosely correlated, we get a non-negligible power dependence, similar to those reported in the above mentioned references [4-6, 26-28]: $\bar{n}_{det}(10^{20}m^{-3}) \approx 0.51 \times I_p^{0.74\pm0.09} P^{0.31\pm0.07} B_\phi^{-0.45\pm0.09}$. With the caveat that detachment and DL could differ, this result anyway supports a clear DL dependence on P, compatible with our model's prediction.

Other experiments are also quoted in paragraph 2.2.4 of [2]. We briefly comment only those reported alongside a reference, and therefore verifiable. In [30], referring to DITE, it is written that moderate NBI heating increases the DL, but very large NBI heating is less effective. However, this statement is not quantified, nor the figures of that paper allow doing by ourselves this kind of analysis. Reference [31] only cites the above discussed reference [29], as far as the power dependence of L-mode DL is concerned. Finally, mention is made of the ASDEX and ASDEX Upgrade experiments reported in figure 8 of the present paper, where a dependence upon heating power is indeed observed. Our conclusion is that the arguments brought by [2] and [29], in support of the independence of the L-mode DL from P, are not convincing.

6. Conclusions

A refinement of an analytical model of the DL in cylindrical geometry [9] is presented. In the presence of radiation losses, DL is obtained as boundary of the equilibrium states with temperature profile satisfying the conditions $T'(0) = T(a) = 0$, and featuring small values only in the edge region. Schematically, the model separates a high-temperature region from a low-temperature region, the latter referring to an interval $T < T_*$ where emission from light impurities is important. The condition of low temperature values only in the edge is formalized by imposing that the separation radius r_*, defined by $T(r_*) = T_*$, is uniquely determined and close to the wall. There are two important improvement with respect to reference [9]: the first, is that radiation from the high temperature region (plasma bulk) is now included; the second, is that the transport dependence of the DL scaling laws is given in terms of the global energy confinement time, in the place of the edge thermal conductivity. The model provides a rather intuitive DL relation, equation (11), expressed by a combination between input power, radiated power, and energy transport. This turns into a Sudo-like scaling law, equation

(12), when the thermal transport is specialized for the stellarator. We note that (12) was recognized as the correct scaling for the Wendelstein 7-X stellarator [13, 14]. Nonetheless scaling (11) is also the basis for further developments. In particular, by combining it with the on-axis Ohms's law and other MHD relations, a less obvious DL scaling law, equation (17), is obtained for the tokamak and the RFP, featuring an important net dependence on I_p. For purely ohmic configurations it is given by the almost linear factor $I_p^{8/9}$. Moreover, the dependence on thermal transport is negligible ($\tau_E^{-1/9}$), thus providing almost the same DL in the ohmic tokamak and the (ohmic) RFP, as experimentally observed. The unification of the DL description in widely different configurations (stellarator, tokamak, RFP) is a strong point in favor of this model. As far as the additionally heated tokamak is concerned, the current dependence of (17) is weaker, $I_p^{4/9}$, but this is compensated for the explicit power dependence $P^{4/9}$, not present in the ohmic case. Relation (17) should be representative of the L-mode tokamak, since the pedestal physics ruling the H-mode, is not included in this basic model. An alternative scaling for L-mode tokamaks, equation (13), is derived directly from (11) by specializing the thermal transport with the empirical ITER89-P scaling law. The resemblance of the two expressions (13) and (17) is explained by the fact that the MHD equations linking (11) to (17) imply dependences on P and I_p, for τ_E at the DL, similar to those of the ITER89-P.

Both scaling (13), (17) have been compared to a set of high-density disrupted L-mode JET discharges, with both additionally heated and purely ohmic shots. With respect to previous validations based on published data [9], here we take advantage of shot-by-shot signals for many quantities. In particular, the measured Z_{eff} provides a sort of average impurity concentration, which is another key parameter of the model, besides P and I_p. Nonetheless, the exact impurity composition, namely the relative concentrations $\hat{f}_j$, which determine the average radiation rate coefficient (2), as well as the concentration of edge neutral particles, whose line emission is taken into consideration, are parameters more difficult to assess. Measured profile parameters for temperature and density are used to estimate, to our best, the profile factors entering the modelled DL scaling laws. Both expressions (13), (17) are compatible with the upper boundary of the observed densities, taking reasonable values of the input quantities, and limiting impurities to the light species C, O, Be, but one shot (87494) where a small amount of W was included. The DL power dependence predicted by the model is confirmed by further discharges, disrupted at nearly constant density soon after the NBI switching off. A simplified version of (17) has been also considered, equation (20), by replacing uncertain terms with typical estimates: in particular, for shape factors and average radiation rate coefficients, we take values *suitable to mildly/weakly peaked density profiles and light impurities*, respectively. Thus, all the dependences, but the neutral effective concentration parameter, reduce to measurable quantities.

The good fit of the maximum densities, achieved by this scaling, confirms that it contains the relevant dependencies. This expression also aligns fairly well published DL data of L-mode experiments performed in different tokamaks. Accordingly, we propose a reinterpretation of figure 9a of [29], reported in [2] to support the DL independence from power in the L-mode tokamak: our counter-analysis shows that a P dependence is instead hidden in the data of this figure. Finally, we point out the inadequacy of the *pure* Greenwald limit $\langle n_e \rangle (10^{20} m^{-3}) = n_G$ as a criterion to interpret the maximum densities observed shot-by-shot, both in the above JET database, and in the considered L-mode published data. In a loose sense, it could be considered an envelope of the JET database, since none of those disruptions occurs at $\langle n_e \rangle > n_G$. Nevertheless, this seems to be more incidental than physically based, since n_G can be also significantly exceeded, by additional heating, as shown in figure 8a, or by density profile peaking, as demonstrated in [32]. There are also other general reasons to doubt the pure Greenwald limit. Its simplicity is captivating (dependences on current and minor radius only), but it unavoidably creates a gap between the tokamak and the RFP from one side, and the stellarator from the other side, where the empirical scaling law features input power as a key dependence. This is a problem, if we imagine that the ultimate DL (not a benign DL as the H→L back-transition) is ruled by some basic mechanism not very sensitive to the details of the configuration. Showing that plasma current can be hosted within a power-balance DL formulation, if complemented by other dependences, the proposed model fills this gap, providing a possible unified description of the phenomenon.

Acknowledgement

We thank P. Vincenzi for providing the NBI shine-through signals, and M. Valisa for helpful discussions, and A. Huber for useful suggestions. We also thank Nick Eidietis for providing us the ITPA disruptions database, from which we take the JET shots discussed in section 3. This work has been carried out within the framework of the EUROfusion Consortium and has received funding from the Euratom research and training programme 2014-2018 and 2019-2020 under grant agreement No 633053. The views and opinions expressed herein do not necessarily reflect those of the European Commission.

Appendix A: atomic data

For main ion (D or He) and impurities we adopt the average charge Z_j and the radiation rate coefficient $Rad_{j,FLYCHK}$ (in erg/s/atom) computed by the FLYCHK code [21]. The choice is motivated by the completeness of the atomic data there accessible: for all elements with Z<80, charge and radiation rate coefficient are given in a wide interval of density and electron temperature ($T = 0.5eV \div$

$100keV$). The Rad_j, here adopted in m^3W units, are obtained from the FLYCHK estimates by the conversion $Rad_j = Rad_{j,FLYCHK} \times 10^{-7}/n_e$. Both $Z_j$and Rad_j are *almost density independent* in the typical range $n_e{\sim}10^{19} \div 10^{20}$ of the plasmas here considered. Hence, they are taken as functions of the temperature only: $Z_j(T),\ Rad_j(T)$. In order to have an order of magnitude of the neutral radiation, we consider the atomic D$_0$ and He$_0$ line emission estimated by FLYCHK: the inclusion of other loss mechanisms is realized through the effective concentration parameter f_0. For tungsten (W) we also consider the estimate listed in table 2 of the paper by T. Putterich et al [22]: here $Z_W(T),\ Rad_W(T)$ are reported within the interval 30eV÷40keV, which excludes the very low temperatures. The radiation rate coefficients of the species considered in the present work are displayed in figure A1.

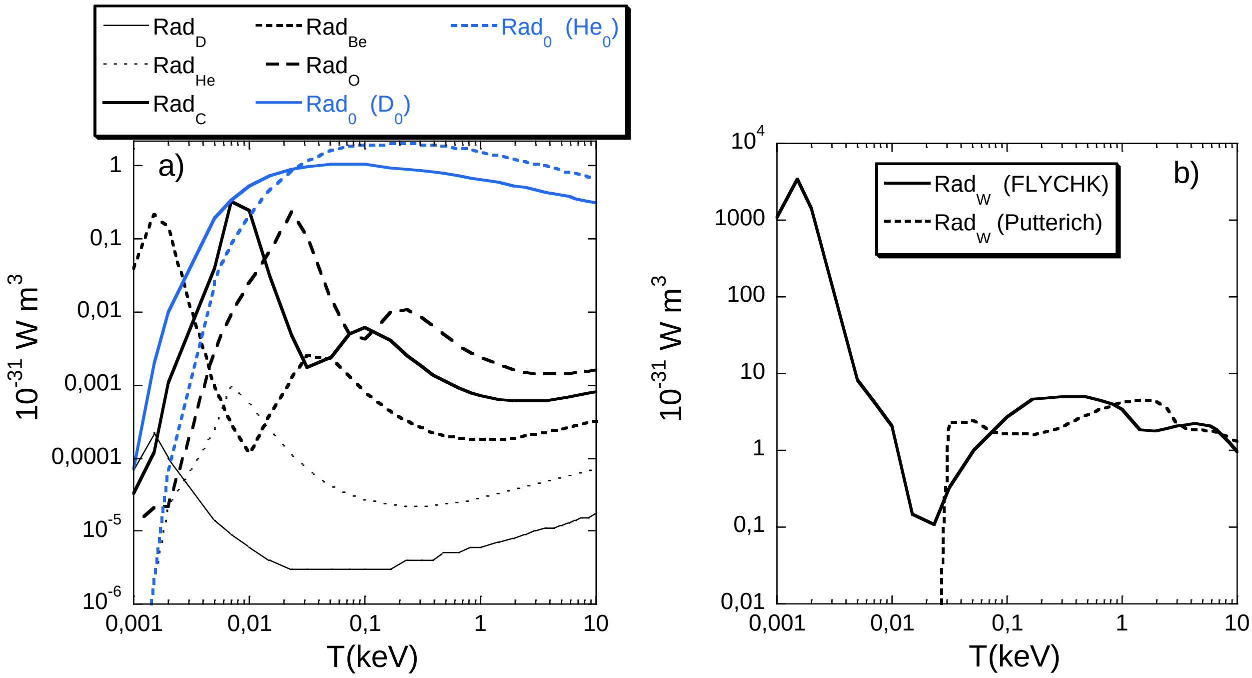

Figure A1. Plot a): radiation rate coefficient of main ions (D, He), light impurities (C, Be, O), and from line emission of neutral atoms. Plot b): same quantity for Tungsten, with estimates from FLYCHK [21] and Putterich [22], the latter excluding the interval $T < 30eV$.

Appendix B: Estimate of the profile factors Ψ_p and Ψ

The analysis is very similar to that presented in Appendixes B and C of [9], and it is based on numerical solution of (1) for the normalized temperature profile $\hat{T} = T/T(0)$. Following the definitions given in (9) we write

$$\text{B1)}\quad d\left(x\hat{K}\, d\hat{T}/dx\right)/dx + \Omega\, x \left[\hat{\wp}(x) - \frac{\int_0^1 dy\, y\, \hat{\wp}}{\int_0^1 dy\, y\, \hat{\mathfrak{R}}}\hat{\mathfrak{R}}(x)\right] = 0, \qquad x = r/a$$

Constant Ω is determined by the condition $\hat{T}(1) = 0$. Note that the DL condition, i.e. total heating power equal to total radiated power, is assumed in (B1). The edge-normalized radiation power density is here modeled by a step-wise function: $\widehat{\Re}(x) = \Re(x)/\Re(x_*) = \{\Re_{bulk}/\Re(x_*),\ x < x_*;\ 1,\ x_* \leq x \leq 1\}$. Accordingly, the radiation shape factor is $\delta_{Rad} = \int_0^1 dxx\widehat{\Re}/\int_{x*}^1 dxx\widehat{\Re} = 1 + \frac{x*^2}{1-x*^2}\frac{\Re_{bulk}}{\Re(x_*)}$. We fix $x_* = 0.9$ throughout this computation. $\widehat{K}$ is written by means of an edge-normalized effective thermal diffusivity: $\widehat{K} = K/K_* \approx (n_e\, \chi_{eff})/[n_*\, \chi_{eff}(a)] = \delta_n \times n_e/n_{bulk} \times \hat{\chi}_{eff}$, being $\hat{\chi}_{eff} = \chi_{eff}/\chi_{eff}(a)$. The different configurations, L-mode tokamak, stellarator and RFP are discussed separately.

L-mode tokamak

We take the model $\hat{\chi}_{eff} = \left[\chi_0^{1/\alpha} + \left(1 - \chi_0^{1/\alpha}\right) \times x^2\right]^{\alpha}$, with $\chi_0 = \hat{\chi}_{eff}(0)$, and $\chi_0 \leq 1$, $\alpha \geq 1$. Therefore, $\hat{\chi}_{eff}$ increases with the radius, in agreement with the experimental transport analysis in this configuration [15]. The on-axis normalized heating power density is split into the ohmic and auxiliary heating contributions. No anomaly factor for the on-axis Spitzer resistivity is taken here. Hence, ξ is just the current-drive function, $\xi = J_\Omega/J$, assumed to be radially constant (this simplification avoids numerical problems in the equations solution):

$$\text{B2)}\quad \hat{\wp} = \wp/\wp(0) = \frac{\xi\, V_\phi I_p\, q(a)/q(0) \times \left(1-x^2\right)^{q(a)/q(0)-1} + P_{aux} \times (p+1) \times \left(1-x^2\right)^p}{\xi\, V_\phi I_p\, q(a)/q(0) + P_{aux} \times (p+1)}$$

The two terms added at the numerators are heating power densities, ohmic and auxiliary respectively, multiplied by the plasma volume. The ohmic term derives from $\eta J_\Omega^2 = \xi\, \eta J_\Omega J \cong \xi E_\phi\, J_\phi$, combined with the standard toroidal current density model $J_\phi = I_p/(\pi a^2) \times q(a)/q(0) \times (1 - x^2)^{q(a)/q(0)-1}$ [16]. The auxiliary heating term is shaped by the profile $(1 - x^2)^p$, and quantified by the total power P_{aux}. The ratio $q(a)/q(0)$ is obtained from $\hat{T}$ by exploiting Ohm's law $E_\phi \approx \xi\eta J_\phi$ and Spitzer's resistivity $\eta \propto T^{-3/2}$:

$$\text{B3)}\quad q(a)/q(0) \approx 0.5 \times \left(\int_0^1 dx\, x\, \hat{T}^{3/2}\right)^{-1}$$

Equations (B1), (B2), (B3) are solved iteratively, by giving ξ, p, $P_{aux}/(V_\phi I_p)$, χ_0, α, $\Re_{bulk}/\Re(x_*)$, alongside the density profile, as input quantities. Then, Ψ_p and Ψ are computed according to the definitions given in equations (10) and (17). A regression analysis finds out negligible their dependence on ξ, p, $P_{aux}/(V_\phi I_p)$, probably because the multiple radial integration involved in these factors weakens the dependence on the $\hat{\wp}$ radial profile. As far as the dependences on χ_0, α, $\Re_{bulk}/\Re(x_*)$, as well as that on density profile, are concerned, we can express them as power law scaling of δ_T, δ_{Rad}, δ_n. In particular,

B4) $\Psi \approx 4.43 \times \delta_T^{0.825}\ \delta_n^{0.166}\delta_{Rad}^{0.387}$

Moreover, the factor entering the scaling (13) is approximated by

B5) $\Psi_p^{-0.345} \approx 2.83 \times \delta_T^{0.529}\ \delta_n^{-0.321}\delta_{Rad}^{0.269}$

Plots (a), (b) of figure B1 give an idea of the goodness of these approximations.

Stellarator

In this case $V_\phi = 0$, and expression (B2) simplifies into $\hat{\wp} = (1 - x^2)^p$. As far as the thermal diffusivity is concerned, we take the non-monotonic radial profile already adopted in [9], and suggested by LHD transport analyses [12]: $\hat{\chi}_{eff} = 4 \times (x - x^2) + 1$. Equation (B1) is solved by giving p, $\Re_{bulk}/\Re(x_*)$, alongside the density profile, as input quantities, and Ψ_p is then computed. The approximation

B6) $\Psi_p^{-0.4} \approx 3.62 \times \delta_T^{0.544}\ \delta_n^{-0.396}\ \delta_{Rad}^{0.375}$

holds for the factor entering scaling (12), as shown by plot (c) in figure B1.

RFP

We do not present a new derivation here, but we rely on the estimate made for a typical RFX-mod equilibrium, presented in Appendix C of reference [9]. Since density and temperature profiles are rather flat there close to the DL, we can approximate $\Psi_p^{\frac{1}{10}} \approx \Im_p^{\frac{1}{10}}$, hence $\Psi \approx \left[J_\phi(0)/\langle J_\phi\rangle\right]^{\frac{2}{5}} \Im_p^{-\frac{1}{2}}$. By exploiting the correspondences, $\Pi_{RFP} \to \psi(a)$ and $\Im_p \times \left[J_\phi(0)/\langle J_\phi\rangle\right]^{-1} \to \widehat{\Im} \times \psi(a)^{-1}$, between the quantities defined in the present paper, and those ($\widehat{\Im}$, $\psi(a)$) used in [9], we can write the product of the shape factors entering (17) in the RFP case as $\Pi_{RFP}^{4/9} \times \Psi^{10/9} \approx \left[J_\phi(0)/\langle J_\phi\rangle\right]^{-\frac{1}{9}}\ \widehat{\Im}^{-\frac{5}{9}}\,\psi(a)$. The estimate of the terms in the r.h.s, done in [9] for an equilibrium with reversal and pinch parameters respectively $F = -0.145$ and $\Theta = 0.143$, gives $\Pi_{RFP}^{4/9} \times \Psi^{10/9} \approx 3.7$.

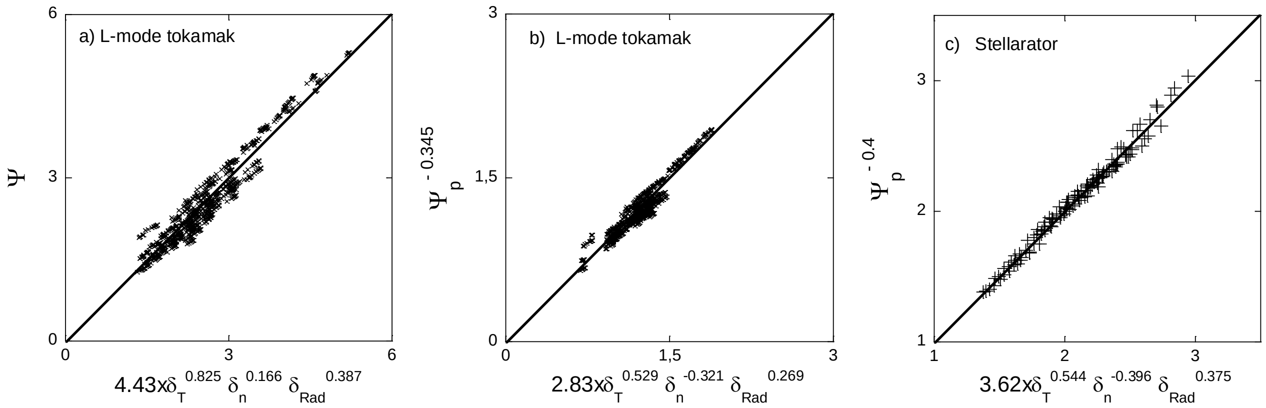

Figure B1. Profile factors vs interpolating scaling laws. Plots (a), (b) refer to the L-mode tokamak. Plot (c) refers to the stellarator.

Appendix C: derivation of scaling (17) from equation (11)

To unify the notation of tokamak and RFP cases, we define $\Pi \in \{\Pi_{tok}, \Pi_{RFP}\}$ and $\mathrm{y}_0 \in \{\xi(0),\ C(0)\}$, where, for both quantities, the first choice is for the tokamak and the second one for the RFP. As explained in paragraph 2.4 we write $P = I_p\, V_\phi/\mathrm{y}_0\ \times \Pi$ or equivalently

C1) $P(MW) = \pi a^2\, n_G\, V_\phi/\mathrm{y}_0\ \times \Pi$

On-axis Ohm's law (14), written as $V_\phi/\mathrm{y}_0 = 0.2 \times \pi\, R_0\, \eta_1\, \zeta\, Z_{eff}\, T_0^{-\frac{3}{2}}\, J_\phi(0)/\langle J_\phi\rangle\, n_G$, is combined with (9) for T_0, (10) for K_*, (C1) for P. Taking into account the Ψ definition given in (17), one gets:

C2) $V_\phi/\mathrm{y}_0 = 0.129 \times \pi\, R_0\, \left[\eta_1\, \zeta\, Z_{eff}\right]^{2/5} n_G^{-\,1/5}\, n_*(10^{20})^{3/5}\, (\tau_E\, \Pi\,)^{-\,3/5}\, \Psi\ \Psi_p^{1/2}$

Then, (C2) is inserted into (C1), giving:

C3) $P(MW) = 0.129 \times \pi^2 a^2 R_0\, \left[\eta_1\, \zeta\, Z_{eff}\, \Pi\right]^{2/5} n_G^{4/5}\, n_*(10^{20})^{3/5}\, \tau_E^{-\,3/5}\, \Psi\ \Psi_p^{1/2}$

By inserting (C3) into (11) and making use of the DL relation $n_* = n_1 \times \Theta(\iota)$, one ends up with expression (17)

Appendix D: approximate relation between T_* and the edge temperature gradient

Taking into account that $T(a) = 0$, the Taylor expansion of $T(r)$about $r = a$,

D1) $T(r_*) \approx T'(a)(r_* - a) + T''(a)\,(r_* - a)^2/2,$

is combined with the Taylor expansion about $r = r_*$,

D2) $T(a) = 0 \approx T(r_*) + T'(r_*)(a - r_*) + T''(r_*)\,(a - r_*)^2/2$

One gets

D3) $T(r_*) \approx X(r_* - a) + \ Y\,X'\,(r_* - a)^2/2\,;$

$$X = [T'(a) + T'(r_*)]/2\,; \quad X' = [T''(a) + T''(r_*)]/2\,; \quad Y = [T''(a) - T''(r_*)]/[T''(a) + T''(r_*)]$$

Now we consider equation (1) in $[r_*,\ a]$. Since $r_* \approx a$, $K(r_*) \approx K(a)$, and $\wp \ll \Re$ in this interval, one can approximate $Y \approx [\Re(a) - \Re(r_*)]/[\Re(a) + \Re(r_*)]$. By assuming that the *variation* of $\Re$ within $[r_*,\ a]$ is much smaller than $\Re$ itself, one ends up with $Y \ll 1$, hence $T(r_*) \approx X(r_* - a)$.

References

[1] S. Sudo et al, Nucl. Fusion **30** (1990) 11

[2] M. Greenwald, Plasma Phys. Contr. Fusion **44** (2002) R27

[3] M. Valisa *et al*, Fusion Energy 2004, Proc. 20th Int. Conf. Villamoura, 1-6 November 2004 (Vienna: IAEA) [EX/P4-13], http://www-naweb.iaea.org/napc/physics/fec/fec2004/datasets/index.html

[4] A. Stabler et al, Nucl. Fusion **32** (1992) 1557

[5] G. Duesing and the JET Team, Plasma Phys. Contr. Fusion **28** (1986) 1429

[6] A.Huber et al, J. Nucl. Mater. **438** (2013) S139

[7] A.Huber et al, Nucl. Fusion **57** (2017) 086007

[8] M. Bernert et al, Plasma Phys. Contr. Fusion **57** (2015) 014038

[9] P. Zanca et al, Nucl. Fusion **57** (2017) 056010

[10] S. I. Braginskii, 'Transport processes in a plasma', *Reviews of Plasma Physics* (Consultants Bureau, New York, 1965), Vol. 1, pag. 205-311.

[11] J. Freidberg, 'Plasma Physics and Fusion Energy', Cambridge University Press, New York (2007)

[12] S. Inagaki et al, Nucl. Fusion **46** (2006) 133

[13] G. Fuchert *et al*, 2017 European Conference on Circuit Theory and design (ECCTD), 4-6 September 2017, Catania, Italy, https://ieeexplore.ieee.org/stamp/stamp.jsp?tp=&arnumber=8093228

[14] G. Fuchert *et al*, 27th IAEA Fusion Energy Conference, 22-27 October 2018, Gandhinagar, India, EX/3-5, https://conferences.iaea.org/indico/event/151/papers/6106/files/4761-iaea_template_fuchert.pdf

[15] ITER Physics Expert Group on Confinement and Transport et al, Chapter 2: Plasma confinement and transport, Nucl. Fusion **39** (1999) 2175

[16] J. A. Wesson, '*Tokamaks*', 3rd edition (2004) (Oxford: Clarendon)

[17] S. Cappello, D. Bonfiglio, D. F. Escande, Phys. Plasmas **13** (2006) 056102

[18] G. Spizzo *et al*, Nucl. Fusion **55** (2015) 043007

[19] M. E. Puiatti *et al*, Phys. Plasmas **16** (2009) 012505

[20] K. Thomsen et al, Nucl. Fusion **34** (1994) 131

[21] Atomic Molecular Data Services, https://www-amdis.iaea.org/FLYCHK/

[22] T. Putterich et al, Nucl. Fusion **50** (2010) 025012

[23] M. Groth et al, Nucl. Fusion **53** (2013) 093016

[24] S. Brezinsek et al, J. Nucl. Mater. **463** (2015) 11-21

[25] P. Zanca et al, 27th IAEA Fusion Energy Conference, 22-27 October 2018, Gandhinagar, India, TH/P5-22, https://conferences.iaea.org/indico/event/151/papers/6423/files/4556-zanca_iaea_TH_P5_22_rev2.pdf

[26] J. Rapp et al, Nucl. Fusion **39** (1999) 765

[27] Y. Kamada *et al*, *Nucl. Fusion* **31** (1991) 1827

[28] V. Mertens *et al*, *Nucl. Fusion* **37** (1997) 1607

[29] T. W. Petrie *et al*, *Nucl. Fusion* **33** (1993) 929

[30] Axon K B *et al* 1981 *Proc. 8th International Conf. on Plasma Physics and Controlled Nuclear Fusion Research (Brussels, 1980)* vol 1 (Vienna: IAEA) pp 413–423

[31] Maingi R *et al* 1998 *Proc. 17th IAEA Fusion Energy Conf. (Yokohama, 1998)* vol 2, p 793

[32] G. Pucella et al, Nucl. Fusion **53** (2013) 083002